AD-A167 924 PLASMA WAVE OBSERVATIONS AT URANUS FROM VOYAGER 2(U) 1/1
IOWA UNIV IOWA CITY DEPT OF PHYSICS AND ASTRONOMY
D A GURNETT ET AL. 26 MAR 86 U. OF IOWA-86-16
UNCLASSIFIED N00014-85-K-0404 F/G 3/2 NL

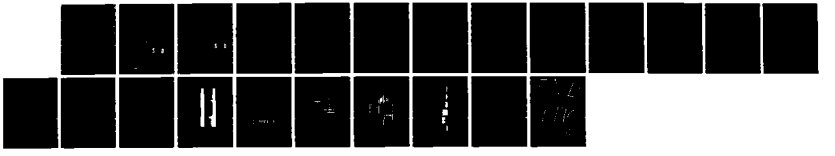

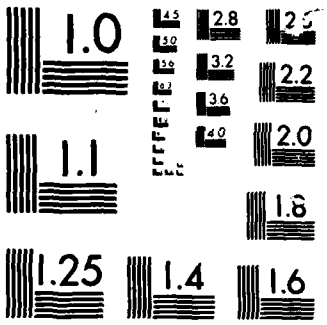


MICROCOPY CHART

U. of Iowa 86-16

(12)



# PLASMA WAVE OBSERVATIONS AT URANUS FROM VOYAGER 2

by

D. A. Gurnett[1], W. S. Kurth[1],
F. L. Scarf[2] and R. L. Poynter[3]




Department of Physics and Astronomy
THE UNIVERSITY OF IOWA
Iowa City, Iowa 52242



86 5 20 023

(12)

U. of Iowa 86-16

# PLASMA WAVE OBSERVATIONS AT URANUS FROM VOYAGER 2

by

D. A. Gurnett[1], W. S. Kurth[1],
F. L. Scarf[2] and R. L. Poynter[3]

February 1986



Submitted to Science.

[1] Department of Physics and Astronomy, The University of Iowa, Iowa City, Iowa 52242

[2] TRW Space and Technology Group, One Space Park, Redondo Beach, California 90278

[3] Jet Propulsion Laboratory, California Inst. of Technology, Pasadena, California 91109

UNCLASSIFIED

SECURITY CLASSIFICATION OF THIS PAGE (When Data Entered)

| REPORT DOCUMENTATION PAGE | | READ INSTRUCTIONS BEFORE COMPLETING FORM |
|---|---|---|
| 1. REPORT NUMBER<br>U. of Iowa 86-16 | 2. GOVT ACCESSION NO. | 3. RECIPIENT'S CATALOG NUMBER |
| 4. TITLE (and Subtitle)<br>PLASMA WAVE OBSERVATIONS AT URANUS FROM VOYAGER 2 | | 5. TYPE OF REPORT & PERIOD COVERED<br>Progress February 1986 |
| | | 6. PERFORMING ORG. REPORT NUMBER |
| 7. AUTHOR(s)<br>D. A. Gurnett, W. S. Kurth, F. L. Scarf and R. L. Poynter | | 8. CONTRACT OR GRANT NUMBER(s)<br>N00014-85-K-0404 |
| 9. PERFORMING ORGANIZATION NAME AND ADDRESS<br>Department of Physics and Astronomy<br>The University of Iowa<br>Iowa City, IA 52242 | | 10. PROGRAM ELEMENT, PROJECT, TASK AREA & WORK UNIT NUMBERS |
| 11. CONTROLLING OFFICE NAME AND ADDRESS<br>Electronics Program Office<br>Office of Naval Research<br>Arlington, VA 22217 | | 12. REPORT DATE<br>26 March 1986<br>13. NUMBER OF PAGES<br>19 |
| 14. MONITORING AGENCY NAME & ADDRESS(if different from Controlling Office) | | 15. SECURITY CLASS. (of this report)<br>UNCLASSIFIED<br>15a. DECLASSIFICATION/DOWNGRADING SCHEDULE |

16. DISTRIBUTION STATEMENT (of this Report)

Approved for public release; distribution is unlimited.

17. DISTRIBUTION STATEMENT (of the abstract entered in Block 20, if different from Report)

18. SUPPLEMENTARY NOTES

To be published in Science.

19. KEY WORDS (Continue on reverse side if necessary and identify by block number)

Uranus
Plasma Waves
Radio Emissions

20. ABSTRACT (Continue on reverse side if necessary and identify by block number)

(See following page)

DD FORM 1 JAN 73 1473 EDITION OF 1 NOV 65 IS OBSOLETE
S/N 0102-LF-014-6601

UNCLASSIFIED
SECURITY CLASSIFICATION OF THIS PAGE (When Data Entered)

Abstract. Radio emissions from Uranus were detected by the Voyager 2 plasma wave instrument about 5 days before closest approach at frequencies of 31.1 and 56.2 kHz. The bow shock was identified by an abrupt broadband burst of electrostatic turbulence about 10 hours before closest approach at a radial distance of 23.5 $R_U$. Once inside of the magnetosphere strong whistler-mode hiss and chorus emissions were observed at radial distances less than about 8 $R_U$, in the same region where the energetic particle instruments detected intense fluxes of energetic electrons. A variety of other plasma waves, such as $3f_c/2$ electron cyclotron waves, were also observed in this same region. At the ring plane crossing the plasma wave instrument detected a large number of impulsive events that are interpreted as impacts of micron-sized dust particles on the spacecraft. The maximum impact rate was about 20 to 30 impacts/sec, and the north-south thickness of the impact region was about 4,000 km.

The Voyager 2 flyby of Uranus on January 24, 1986, revealed that Uranus has a large and highly unusual magnetosphere. In this paper we present an overview of the principal results from the plasma wave instrument, starting with the first detection of radio emissions from Uranus, and ending a few days after closest approach. To provide a framework for organizing the observations, the results are grouped into related topics, ordered more or less according to the sequence in which the observations were made. For a description of the Voyager plasma wave instrument, see Scarf and Gurnett (1).

Radio Emissions. Since radio emissions escaping from the magnetosphere were expected to provide the first clear indication of a planetary magnetic field (2), the detection of radio bursts was an important objective as Voyager approached Uranus. In contrast to Jupiter and Saturn, radio emissions were not observed until the spacecraft was very close to the planet. The first clear radio emissions from Uranus were detected by the plasma wave instrument on January 19, 1986, only about 5 days before closest approach. At this time Voyager was at a radial distance of about 275 Uranian radii ($R_U$) from Uranus. This first radio emission is illustrated in Fig. 1, which shows the intensities in two frequency channels, 31.1 and 56.2 kHz. The emission is strongest in the 31.1-kHz channel, and highly variable, with numerous sporadic bursts on time scales of seconds and minutes. Sporadic emissions of this type are apparently quite rare, because several days elapsed before another comparable radio burst was detected.

A second type of radio emission was detected a few days later, about 18 hours before closest approach. This radio emission has much smoother temporal variations and can be seen in the four-day overview plot of Fig. 2 at 17.8, 31.1 and 56.2 kHz. The emission exceeded the receiver noise level at about 40 $R_U$ on the inbound pass, reached maximum intensity near closest approach, at about 1800 spacecraft event time (SCET) on January 24, and dropped below the receiver noise level at about 40 $R_U$ on the outbound pass. This same radio emission was also detected up to much higher frequencies, approximately 800 kHz, by the planetary radio astronomy experiment (3). Because of the smooth spectrum and slow temporal variations, this radio emission appears to be similar to escaping continuum radiation at Earth (4).

A third type of radio emission was detected during the outbound pass on the nightside of Uranus. This radio emission is composed of numerous very narrow bandwidth (few %) components centered around 5 kHz, and can be seen in the 5.62-kHz channel on January 25 and 26 (see Fig. 2). This narrowband emission varies sporadically on time scales as short as a few seconds and was detected on and off for about 6 days after closest approach. The frequency is well above the local electron plasma frequency, so the waves must be propagating in the free space electromagnetic mode. Although not as steady, the radiation has many similarities to the narrowband electromagnetic emissions observed at Jupiter and Saturn (5). The Jovian and Saturnian narrowband emissions are believed to be produced by mode conversion from electrostatic waves near the electron cyclotron frequency (6). If the narrowband emissions from Uranus are generated at a frequency near the electron cyclotron frequency, then based on the magnetic field model provided by the magnetometer team (7) the source would be located at a radial distance near the orbit of the moon Miranda.

Upstream Waves, Bow Shock and Magnetopause. The first clear evidence of upstream waves associated with the bow shock of Uranus occurred at 0550 SCET on January 23, when a strong burst of electron plasma oscillations was detected in the 1.78-kHz channel. These waves are produced by electrons escaping into the solar wind from the bow shock and are a well-known feature of the upstream solar wind at Earth, Jupiter and Saturn (8). Electron plasma oscillations occurred on and off for about a day until the spacecraft finally crossed the bow shock at 0728 SCET on January 24, at a radial distance of about 23.5 $R_U$. The plasma wave intensities near the shock are shown in Fig. 3. The bow shock is easily

identified in these data by the abrupt broadband burst of electrostatic turbulence from about 0728 to 0735 SCET. The location of the shock is consistent with the shock identified by the magnetometer (7) and plasma (9) instruments. Although the solar wind density is unusually high, the overall characteristics of the electrostatic turbulence are very similar to other planetary bow shocks (10). Plasma wave turbulence is believed to play an important role in energy dissipation at collisionless shocks.

Downstream of the shock the electric field intensities dropped to very low levels throughout the magnetosheath, very similar to Jupiter and Saturn. The magnetometer data show that the magnetopause, which marks the entry into the magnetosphere, occurred at 1007 SCET (7). The only observable plasma wave effect at the magnetopause is a slight increase in the electric field intensities at 1.78 kHz. This increase is apparently due to electromagnetic radiation trapped in the low density cavity formed by the magnetosphere, similar to the trapped continuum radiation at Jupiter (11).

Magnetosphere. After crossing the magnetopause the plasma wave intensities remained relatively low until the spacecraft reached the inner region of the magnetosphere at radial distances less than about 8 $R_U$. A 16-channel plot of the plasma wave intensities in the inner region of the magnetosphere is shown in Fig. 4. The electron cyclotron frequency is indicated by the solid line, which was derived from a model provided by the magnetic field investigators (7). The electron cyclotron frequency is given by $f_c = 28\ B$ Hz, where B is the magnetic field strength in nanoteslas. The inner magnetosphere is characterized by strong whistler-mode emissions. These emissions occur below the electron

cyclotron frequency and extend almost continuously from about 1520 SCET on the inbound pass, through the region near closest approach, to about 2110 SCET on the outbound pass. The identification of these waves as whistler-mode emissions is based on the frequency range, which is always below the electron cyclotron frequency, and on comparisons of wideband spectrograms with similar spectrograms at Earth, Jupiter and Saturn. To illustrate these comparisons, six 10-second spectrograms of the wideband data are shown in Fig. 5. These "snapshots" were obtained from short segments of the electric field waveform that were digitized at a high rate (28,800 samples/sec) on the spacecraft, transmitted to the ground, then Fourier transformed to produce spectrograms. The labels A through F indicate the location of each of the spectrograms in Fig. 4. Spectrograms A, B, C and F show a type of whistler-mode emission known as hiss. Whistler-mode hiss has relatively little spectral structure and occurs in the plasmasphere at Earth, in the Io plasma torus at Jupiter and in the magnetosphere of Saturn (12). Spectrogram B shows another type of whistler-mode emission known as chorus. Chorus consists of many discrete tones, usually rising in frequency with increasing time, and also occurs in the magnetospheres of Earth, Jupiter and Saturn (13).

Chorus and hiss are both believed to be produced by cyclotron resonance interactions with energetic electrons. The free energy source comes from the anisotropy produced by the loss cone in the trapped electron distribution. For many years whistler-mode emissions have been thought to play an important role in planetary radiation belts because they cause pitch-angle scattering, eventually precipitating the particles into the atmosphere. Because the wave intensities increase rapidly as

the number of resonant particles increases this loss mechanism limits the maximum electron flux in the radiation belt (14). The electron precipitation into the atmosphere can also produce auroral light emissions.

It is useful to estimate the resonance energies for the whistler-mode emissions observed in the magnetosphere of Uranus. For the chorus emissions in spectrogram B at 1802 SCET the electron resonance energy for parallel propagation is about 240 keV, assuming an electron density of about 0.4 $cm^{-3}$. This electron density is based on preliminary estimates from the plasma instrument (9). For the hiss in spectrogram F at 2035 SCET the electron resonance energy is about 60 keV, assuming an electron density of 0.3 $cm^{-3}$. In both cases the resonance energies are in a region of the energy spectrum where the energetic charged particle instrument detected intense fluxes of trapped electrons (15). These electrons presumably provide the free energy source for the waves. The hiss emission became particularly intense on the outbound pass near 2000 SCET (see Fig. 4), with maximum broadband electric field amplitudes of 1.9 mV/m. The reason for the intensification in this region is not known, since comparable intensities were not observed on the same L-shells on the inbound pass. In any case the large wave intensities should produce rapid pitch-angle scattering and precipitation of trapped electrons, thereby possibly accounting for the UV emissions observed on the nightside of Uranus (16).

In addition to the whistler-mode emissions a variety of other plasma waves were observed in the inner magnetosphere. On the inbound pass strong emissions can be seen in the 1.00- and 1.78-kHz channels from about 1240 to 1320 SCET (see Fig. 2), slightly above the electron

cyclotron frequency. These emissions are almost certainly electrostatic $3f_c/2$ electron cyclotron waves, similar to the electrostatic electron cyclotron waves observed at Earth, Jupiter and Saturn (17). Two other unusual types of emissions can be seen at frequencies from a few hundred Hz to about one kHz in spectrograms D and E of Fig. 6 at 1920 and 1947 SCET. Inspection of the 16-channel plot in Fig. 4 shows that the entire region from about 1910 to 1930 SCET has many intense bursts similar to those in spectrogram D. This region is also remarkably devoid of whistler-mode hiss. At present we have no clear identification of the plasma wave mode responsible for these bursts. Comparison with the magnetic field (7) and energetic particle data (15) suggests that this region may be associated with the Miranda L-shell.

The outbound pass through the magnetotail was characterized by very low plasma wave intensities. The only clearly identifiable plasma wave emissions were at frequencies below 100 Hz from about 0130 to 0330 SCET on January 25 (see Fig. 2). The outbound magnetopause crossing was also very quiet. Several shock crossings were observed during the outbound pass, all with characteristics similar to Fig. 3. After exiting the magnetosphere sporadic bursts of electron plasma oscillations were observed in the solar wind for a period of several weeks. These waves are believed to be caused by electrons streaming outward away from the shock along the interplanetary magnetic field.

Ring plane. As the spacecraft passed through the ring plane at about 1715 SCET on January 24, an intense burst of low frequency noise was observed, centered almost exactly on the ring plane crossing. This noise, which lasted about 6 minutes, can be seen in Fig. 4 at frequencies

below about 1 kHz, increasing in intensity with decreasing frequency. The characteristics of this noise are very similar to those associated with the Voyager 2 ring plane crossing at Saturn, where we detected many small micron-sized dust particles striking the spacecraft (18). Investigation of the wideband data at the Uranus ring plane confirms that the noise is caused by dust impacts. An example of the waveform from the wideband receiver is shown in Fig. 6. The waveform is seen to consist of short impulses, lasting a few milliseconds, very similar to the dust impacts at Saturn. At the time of maximum intensity, around 1715:30 SCET, a preliminary estimate indicates that the impact rate is about 20 to 30 impacts/sec.

As presently understood, the impulsive voltage produced by a dust impact is caused by the charge released when a particle strikes the spacecraft. Laboratory measurements (19) show that when a small particle strikes a solid surface at a high velocity the particle is instantly vaporized and ionized, producing a small cloud of plasma that expands away from the impact site. As the plasma cloud sweeps over the electric antenna, some of the charge is collected by the antenna, thereby causing a voltage pulse. Laboratory measurements show that the charge released is directly proportional to the mass of the particle. The pulse amplitude is therefore proportional to the mass.

Since Voyager 2 passed through the ring plane at about 4.5 $R_U$, well beyond the visible rings, the dust impacts detected by the plasma wave instrument are not directly associated with the rings. It is possible, of course, that these dust particles may represent a disk-like extension of the visible ring system out to where Voyager crossed the ring plane.

Miranda could be another possible source. Based on the similarity to the dust impacts at Saturn, the impacts detected at Uranus are probably caused by particles in the micron size range. Further analysis will be needed to determine an accurate mass and size distribution. The number density, n, can be estimated from the relation R = nUA, where R is the counting rate, U is the spacecraft speed, and A is the area of the spacecraft. Using nominal values, the maximum number density is about $10^{-3}$ particles/$m^3$. From the duration we estimate the north-south thickness, L, of the dust impact region to be about 4,000 km. The columnar number density, nL, is then on the order of a few thousand particles/$m^2$. For micron-sized particles this number density is probably too small to be detected with the imaging system.

## References and Notes


1. F. L. Scarf and D. A. Gurnett Space Sci. Rev. 21, 289 (1977).
2. Possible magnetospheric radio emissions from Uranus were reported by L. W. Brown Astrophys. J. 207, L209 (1976), using data from an earth-orbiting spacecraft.
3. J. W. Warwick et al. Science, this issue.
4. D. A. Gurnett J. Geophys. Res. 80, 2751 (1975); W. S. Kurth, D. A. Gurnett and R. R. Anderson ibid. 86, 5519, (1981).
5. J. W. Warwick et al. Science 204, 995 (1979); D. A. Gurnett, W. S. Kurth and F. L. Scarf ibid. 212, 235 (1981); D. A. Gurnett, W. S. Kurth and F. L. Scarf Nature 292, 733 (1981); F. L. Scarf et al. Science 215, 587 (1982).
6. D. A. Gurnett and L. A. Frank J. Geophys. Res. 81, 3875 (1976); D. Jones Nature 260, 686 (1976); D. B. Melrose J. Geophys. Res. 86, 30 (1981).

7. N. Ness et al. Science this issue.

8. F. L. Scarf et al. J. Geophys. Res. 76, 5162 (1971); F. L. Scarf, D. A. Gurnett and W. S. Kurth Science 204, 991 (1979); D. A. Gurnett, W. S. Kurth and F. L. Scarf ibid. 212, 235 (1981).

9. H. Bridge et al. Science this issue.

10. F. L. Scarf, D. A. Gurnett and W. S. Kurth Nature 292, 747 (1981).

11. F. L. Scarf, D. A. Gurnett and W. S. Kurth Science 204, 991 (1979).

12. R. M. Thorne et al. J. Geophys. Res. 78, 1581 (1973); F. L. Scarf, D. A. Gurnett and W. S. Kurth Science 204, 991 (1979); D. A. Gurnett, W. S. Kurth and F. L. Scarf Science 212, 235 (1981).

13. R. A. Helliwell Whistlers and Related Ionospheric Phenomena Stanford Univ. Press, Stanford, CA, p. 207, (1965); F. V. Coroniti et al. Geophys. Res. Lett. 7, 45 (1980); D. A. Gurnett, W. S. Kurth and F. L. Scarf Science 212, 235 (1981).

14. C. F. Kennel and H. E. Petschek J. Geophys. Res. 71, 1 (1966).

15. S. M. Krimigis et al. Science, this issue.

16. A. L. Broadfoot et al. Science, this issue.

17. C. F. Kennel et al. J. Geophys. Res. 75, 6136 (1970); F. L. Scarf, D. A. Gurnett and W. S. Kurth Science 204, 991 (1979); D. A. Gurnett, W. S. Kurth and F. L. Scarf ibid. 212, 235 (1981).

18. F. L. Scarf et al. Science 215, 587 (1982); Gurnett et al. Icarus 53, 236 (1983).

19. H. Fechtig, E. Grün and J. Kissel Cosmic Dust, ed. J. A. M. McDonnell, Wiley, N. York, 607 (1978).

20. We wish to express our thanks to the Voyager team at the Jet Propulsion Laboratory (JPL) and to the staff at NASA Headquarters for their valuable support. We are especially grateful to E. Miner for his efforts in scheduling the wideband coverage and J. Anderson, C. Avis and the staff of the Multimission Image Processing Laboratory

for their assistance with the wideband data processing. We thank N. Toy and the General Science Data Team for the timely and efficient production of quick-look data products. We acknowledge the full cooperation and support of the Planetary Data System for the use of its facilities, and also the Space Physics Analysis Network for use in communicating data between Iowa and JPL. We also acknowledge the excellent programming support provided by S. Chang and K. Jordan of TRW, and by R. Brechwald, L. Granroth, J. Cook-Granroth and R. Kraemer of the University of Iowa. We also thank N. Ness, S. M. Krimigis, H. Bridge and J. Warwick for their helpful discussions and data comparisons. We remember C. Stembridge for his dedication to the excellence of the Voyager mission and his continual support of the plasma wave investigation. The research at the University of Iowa was supported by NASA through contract 954013 with JPL, grants NGL-16-001-043 and NGL-16-001-002 with NASA Headquarters, by the Office of Naval Research through contract N00014-85-K-0404, and by the State of Iowa through a faculty development assignment for one of the authors (D. Gurnett). The research at TRW was supported by NASA through contract 954012 with JPL.

## Figure Captions

Fig. 1. The first radio emission from Uranus detected by Voyager 2. The spacecraft at this time was at a radial distance of about 275 $R_U$. The instrument noise level is about $10^{-18}$ watts $m^{-2}$ Hz. This threshold is somewhat uncertain because of a problem in the spacecraft data system.

Fig. 2. A 16-channel overview plot of the electric field intensities from the plasma wave instrument. This 4-day plot covers the period from shortly before the inbound shock crossing to shortly after the first outbound shock crossing. The solid line labeled $f_c$ gives the electron cyclotron frequency, computed from a model provided by the magnetic field investigators (7).

Fig. 3. An expanded scale plot showing upstream electron plasma oscillations and the burst of plasma wave turbulence at the inbound shock crossing.

Fig. 4. A 16-channel plot showing the electric field intensities in the inner region of the magnetosphere. The broad region of noise below the electron cyclotron frequency, $f_c$, is caused by whistler-mode emissions. The intense burst of low frequency noise at about 1715 SCET is caused by dust impacts.

Fig. 5. A series of wideband frequency-time spectrograms for selected regions in Fig. 4. Hiss and chorus are both whistler-mode emissions. The plasma wave mode responsible for the emissions in spectrograms D and E have not been identified.

Fig. 6. A voltage waveform from the wideband receiver showing two dust impacts detected near the ring plane crossing.

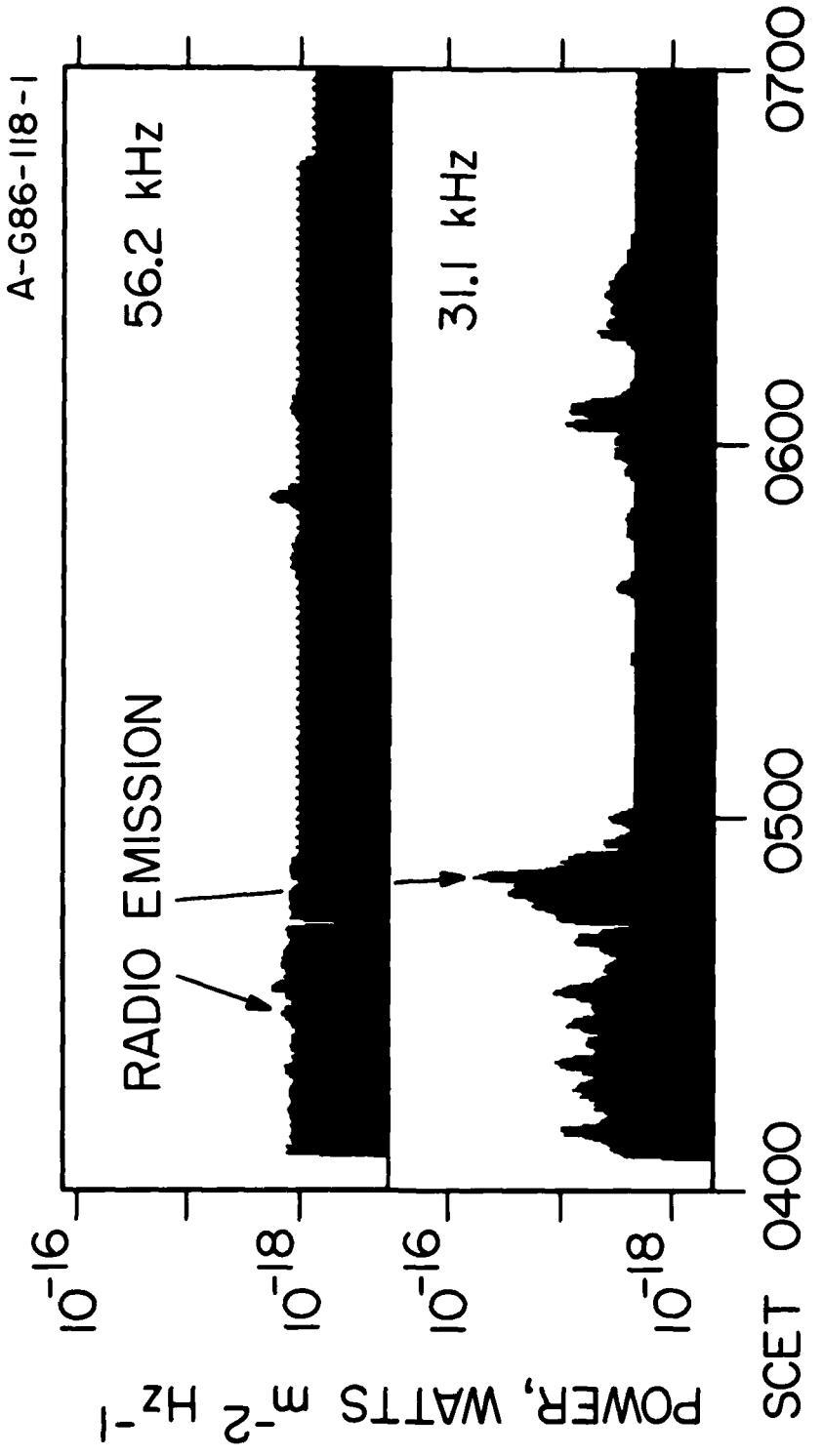
A-G86-118-1
56.2 kHz
31.1 kHz
RADIO EMISSION
POWER, WATTS m⁻² Hz⁻¹
10⁻¹⁶
10⁻¹⁸
10⁻¹⁶
10⁻¹⁸
SCET 0400
0500
0600
0700
JANUARY 19, 1986

Figure 1

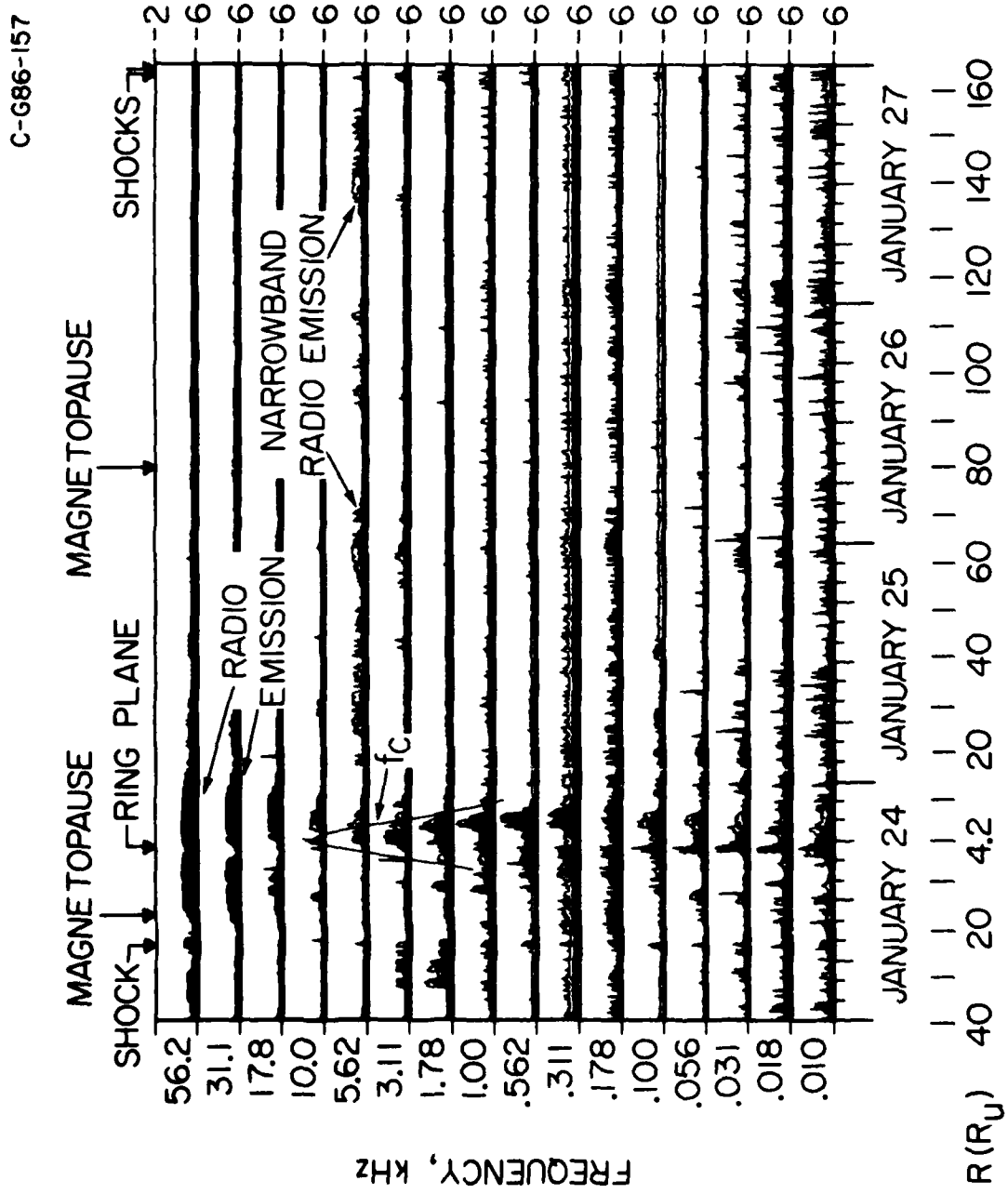
C-G86-157
SHOCK
MAGNETOPAUSE
RING PLANE
MAGNETOPAUSE
SHOCKS
RADIO EMISSION
NARROWBAND RADIO EMISSION
$f_c$
FREQUENCY, kHz
56.2
31.1
17.8
10.0
5.62
3.11
1.78
1.00
.562
.311
.178
.100
.056
.031
.018
.010
$LOG_{10}$ E, VOLTS/METER
-2
-6
R($R_U$)
40
20
4.2
20
40
60
80
100
120
140
160
JANUARY 24
JANUARY 25
JANUARY 26
JANUARY 27

Figure 2

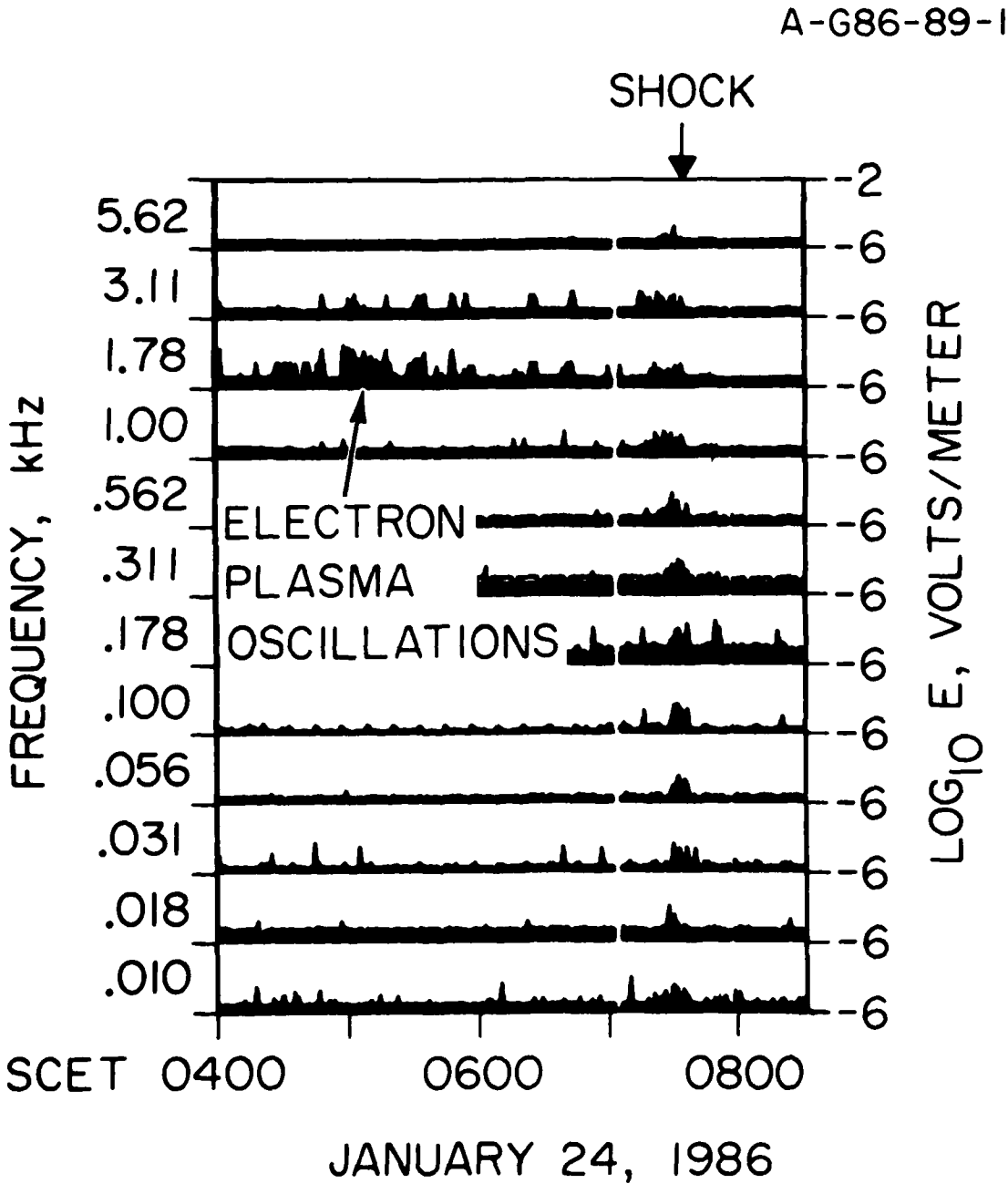
A-G86-89-1
SHOCK
5.62
3.11
1.78
1.00
.562
.311
.178
.100
.056
.031
.018
.010
FREQUENCY, kHz
ELECTRON
PLASMA
OSCILLATIONS
-2
-6
-6
-6
-6
-6
-6
-6
-6
-6
-6
-6
LOG10 E, VOLTS/METER
SCET 0400
0600
0800
JANUARY 24, 1986

Figure 3

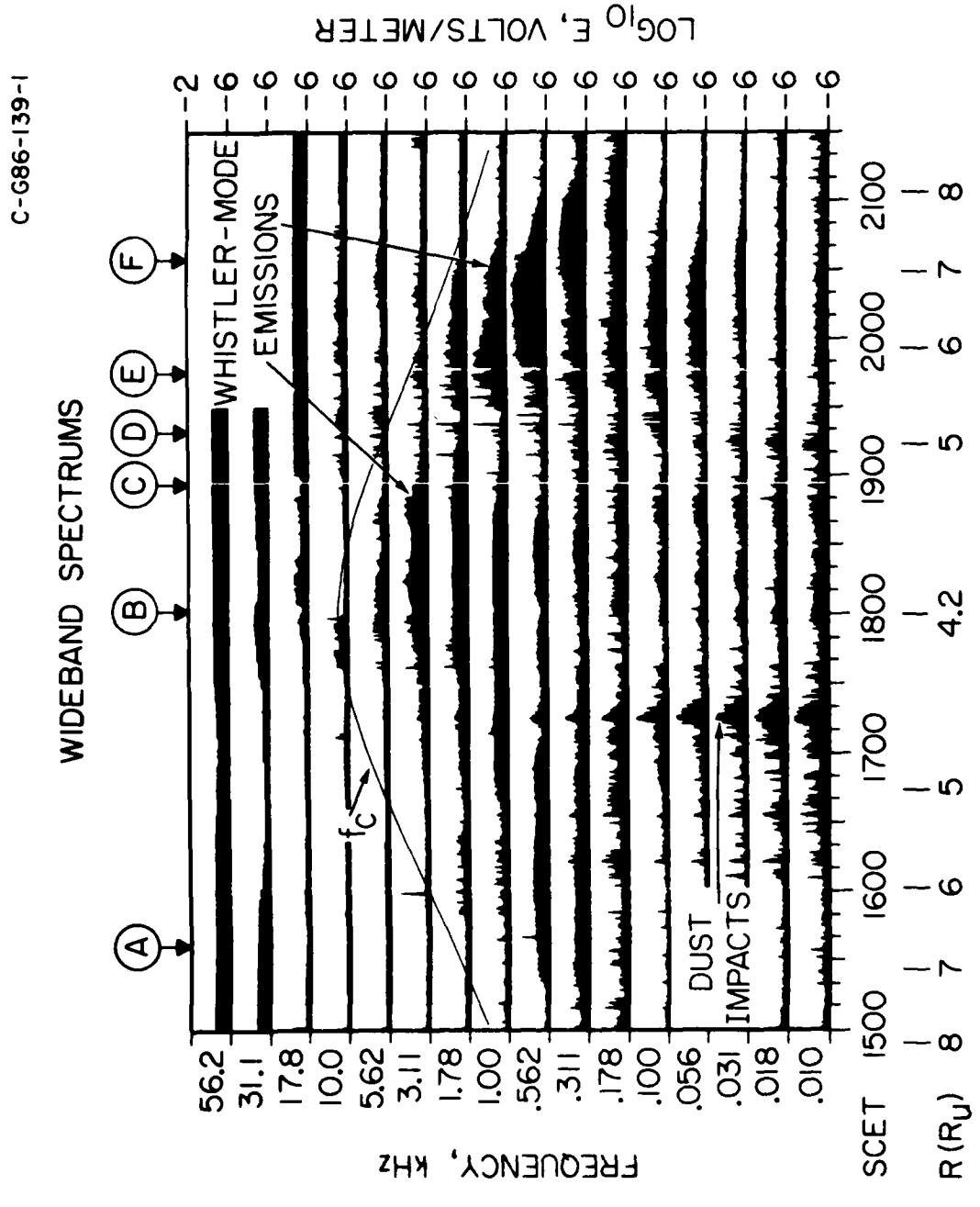
C-G86-139-1
WIDEBAND SPECTRUMS
WHISTLER-MODE EMISSIONS
DUST IMPACTS
$f_C$
A
B
C
D
E
F
FREQUENCY, kHz
56.2
31.1
17.8
10.0
5.62
3.11
1.78
1.00
.562
.311
.178
.100
.056
.031
.018
.010
$LOG_{10}$ E, VOLTS/METER
-2
-6
SCET 1500 1600 1700 1800 1900 2000 2100
R($R_J$) 8 7 6 5 4.2 5 6 7 8
JANUARY 24, 1986

Figure 4

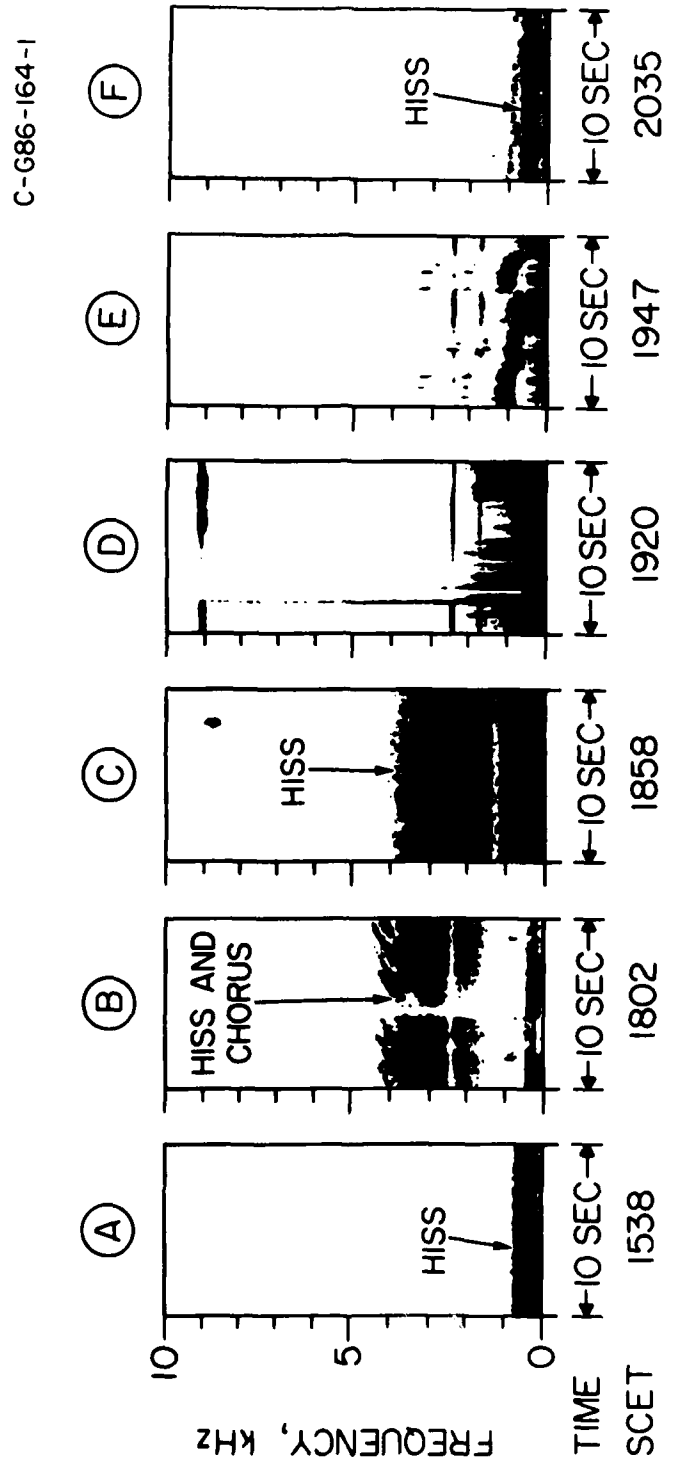
C-G86-164-1
A
B
C
D
E
F
HISS
HISS AND CHORUS
HISS
HISS
10
5
0
FREQUENCY, kHz
TIME
SCET
10 SEC
1538
1802
1858
1920
1947
2035
JANUARY 24, 1986

Figure 5

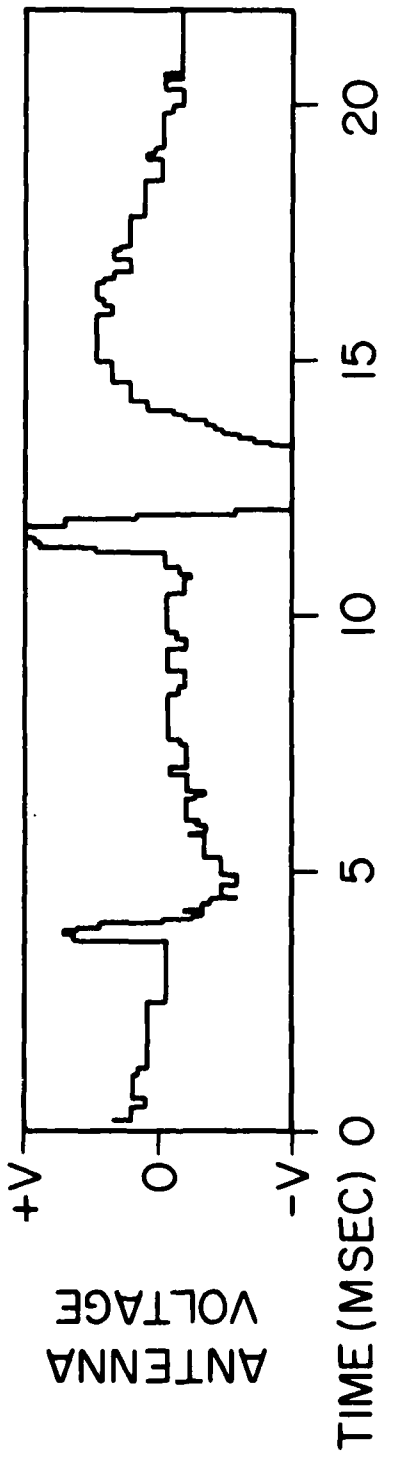
A-G86-155
+V
0
-V
ANTENNA VOLTAGE
0
5
10
15
20
TIME (MSEC)
1716 SCET JANUARY 24, 1986

Figure 6

END

DTIC

6-86